Long-Term Finger Force Predictions Using Motoneuron Discharge Activities

Yuwen Ruan, Long Meng, and Xiaogang Hu

***Abstract*— Surface electromyogram (EMG) signals have been a preferred modality for motor intent detections in the fields of robotic control, rehabilitation, and health monitoring. However, current EMG-based measurement techniques suffer a degradation in performance cross session over time due to factors such as shifts in electrode placement, changes in muscle states, and environmental noise. To address this challenge, we developed a novel neural-drive approach, capable of robust cross-day predictions of individual finger forces. Specifically, high-density EMG (HD-EMG) data were collected from flexor and extensor muscles during single-finger and multifinger tasks. The experimental procedure was repeated three times (sessions), with an average interval of 6.58 days between sessions. We first decomposed the EMG signals in a session to obtain separation matrices that contained motor unit (MU) information in the EMG signals. We then refined the separation matrices that accurately reflected individual fingers. The corresponding separation matrices were applied to EMG signals in the other two sessions to derive the neural drive for force predictions of individual fingers. Our results revealed that the cross-session performance was comparable with the within-session performance. In addition, the neural-drive approach can outperform the conventional EMG-amplitude approach, especially in the cross-session performance. Our developed approach can enhance the long-term reliability of finger force predictions and holds potential for various practical applications.**

***Index Terms*— Cross sessions, finger force measurement, motor unit (MU), neural drive, surface electromyogram (EMG).**

I. Introduction

FINGER force control plays an important role in the daily activities of humans, from grasping objects to performing intricate tasks requiring dexterity and precision [1], [2]. The capacity to perform controlled finger forces is not only fundamental to routine physical interactions but also critical in specialized fields. For example, long-term finger force prediction plays a crucial role in accurate control over assistive robotic hands, such as prostheses or exoskeletons, to achieve smooth and accurate hand movement such as grasping, holding, and manipulating objects [3]. In stroke rehabilitation, long-term monitoring and predicting finger forces can help clinicians to evaluate neuromuscular recovery and adjust the intensity of rehabilitation in a timely manner [4]. In gaming, continuous finger force prediction enables users to manipulate virtual objects with precise finger movements, facilitating the implementation of virtual reality applications [5]. Therefore, finger force predictions have attracted significant interest among researchers seeking to enhance applications in diverse fields such as prosthetic limb interactions [6], [7], rehabilitation [8], [9], and human–machine interactions [10], [11], [12].

Traditionally, finger forces are directly measured using data gloves embedded with integrated force sensors [13], [14]. Although this method offers a direct approach to capturing force data, it comes with drawbacks. The bulky data gloves can restrict natural hand movements, thereby compromising user comfort and the accuracy of force measurement. These limitations have led researchers to explore alternative methods for predicting finger forces.

Finger forces are controlled by neural-drive signals, which are neural commands transmitted from the brain to the muscles and can be decoded from neural signals measured from the brain or muscles [15]. Some previous studies [16], [17], [18] have focused on advancing state-based decoding techniques that identify brain states associated with finger movements to decode finger gesture intentions using electroencephalogram (EEG) signals. However, finger-specific force decoding remains a challenge.

Alternatively, a promising way to decode motion intentions is to use noninvasive surface electromyogram (EMG) signals from the muscles. Compared with EEG signals, EMG signals have shown considerable potential with a considerably high signal-to-noise ratio (SNR) [19], [20]. These signals are generated through the mixture of a large number of motor unit action potentials (MUAPs) across both temporal and spatial domains. Because of the direct correlation between the number of MUAPs at a given time and the intensity of descending neural-drive signals, EMG has been used to interpret motion intentions of distinct gestures [21], [22]. Furthermore, regression analyses have been applied to establish a continuous relation between macroscopic EMG features and finger forces [21], [23]. However, leveraging macroscopic EMG features, such as amplitude, for force prediction faces challenges due to signal crosstalk from adjacent muscle groups, environmental noise, and the inherent dynamic properties of MUAPs, including their superimposition and can-

Received 25 July 2024; revised 22 December 2024; accepted 23 December 2024. Date of publication 10 February 2025; date of current version 19 February 2025. This work was supported in part by the National Science Foundation under Grant CBET-2246162, Grant IIS-2330862, and Grant IIS-2319139; and in part by the Department of Defense under Grant W81XWH2110185. The Associate Editor coordinating the review process was Dr. Nuria Novas. *(Yuwen Ruan and Long Meng contributed equally to this work.) (Corresponding author: Xiaogang Hu.)*

Yuwen Ruan and Long Meng are with the Department of Mechanical Engineering, Pennsylvania State University, University Park, PA 16802 USA (e-mail: yjr5083@psu.edu; lmm7405@psu.edu).

Xiaogang Hu is with the Department of Mechanical Engineering, the Department of Kinesiology, the Department of Physical Medicine and Rehabilitation, the Huck Institutes of the Life Sciences, and the Center for Neural Engineering, Pennsylvania State University, University Park, PA 16802 USA (e-mail: xxh120@psu.edu).

This article has supplementary downloadable material available at https://doi.org/10.1109/TIM.2025.3540139, provided by the authors.

Digital Object Identifier 10.1109/TIM.2025.3540139

cellation. Such factors can bias the prediction of neural-drive signals [24], leading to large estimation errors in finger force predictions. In contrast, advancements in flexible high-density EMG (HD-EMG) electrode recording techniques [25] offer a more refined approach by capturing motor unit (MU) activities at a microscopic level. This approach can track the discharge events of motoneurons, which allows us to predict the descending neural-drive signals based on MU firing spike trains. The firing rates of these MUs, which show a linear relation with neural-drive signals, serve as a detailed microscopic feature for predicting muscle forces [26], [27]. Although promising results have been achieved, current neural-decoding research on force prediction is limited to within-session evaluations. In EMG-related applications, the performance of pretrained models significantly degrades over session and time, primarily due to factors such as variations in EMG characteristics over time, shifts in electrode placement, and varying environmental conditions [19]. These limitations necessitate frequent calibration of the models, which can be inconvenient in practical scenarios, because the computational load is high or data labels may not be available. To address these issues and enhance decoder robustness, it is crucial to establish a robust decoder viable for cross-session force predictions spanned over multiple days, without the need of frequent recalibrations.

Specifically, we acquired HD-EMG data in three different sessions, with an average interval of 6.58 days (±6.47 standard deviation) between sessions, and participants performed either single-finger or multifinger force production tasks. Data from each session served as the training dataset, and the data from the other two sessions were used as the testing dataset. Using the training dataset, we first extracted the MU pool using the fast independent component analysis (FastICA) algorithm. Because it is inevitable that MUs of nontarget fingers are recruited, we refined the MU pool by removing MUs of nontarget fingers. The refined MU pool was then used to predict finger forces across multiple sessions. Our results show that our developed neural-decoding approach can accurately predict single-finger and multifinger forces over different sessions. The key novelty of our study is as follows.

1) We developed a robust neural-decoding approach based on MU firing activity, and we showed that the novel algorithm was capable of robust predictions of individual finger forces across multiple days.
2) Our neural decoder enhanced the stability of EMG-based intent prediction performance, which minimized the need for frequent decoder recalibrations, making our decoder more practical and user-friendly for everyday use.
3) Our decoder was designed to predict dexterous finger motor output at the individual finger and simultaneous multifinger levels, which are essential for daily manual tasks.

II. Methods

Fig. 1 illustrates the framework of the neural-drive-based force prediction. Neural-drive commands were sent from the brain to motoneurons that innervated the finger flexor and extensor muscle compartments. To extract these neural-drive signals, we first obtained the separation matrices containing the MU pool firing information by decomposing the HD-EMG signals of the flexor and extensor muscles. Because the decomposed MU pool contained MUs of different fingers, we refined the separation matrices to isolate MUs specific to the target fingers. We then applied the refined separation matrices directly to HD-EMG data in different sessions. The obtained binary firing events were summed to derive the neural-drive signal. We then predicted the forces of individual fingers using regression functions.

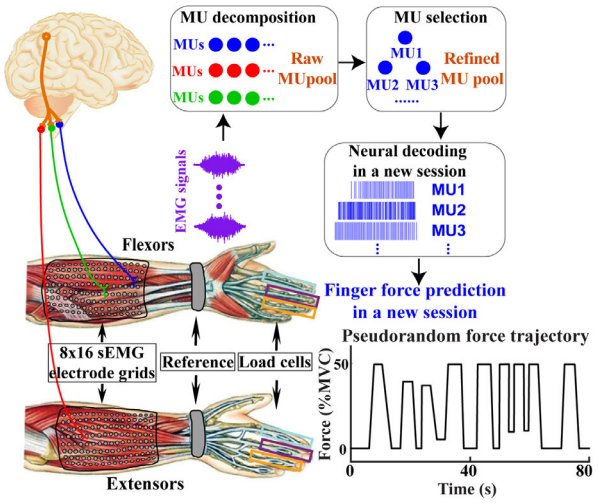

Fig. 1. Overview of the research framework.

A. Data Acquisition

1) Subjects: Eight neurologically intact subjects (five males and three females), aged 21–35, participated in this study, which was approved by the Institutional Review Board at Pennsylvania State University. All subjects provided informed consent in accordance with the approved protocols before the experiment.

2) Experimental Setup: To record EMG signals from the finger flexor and extensor muscles, we used two 8 × 16 electrode arrays with a single-electrode diameter of 3 mm and an interelectrode distance of 10 mm. These arrays were placed on the anterior and posterior sides of the forearm, as shown in Fig. 1. The position of each electrode array was determined by palpating the finger muscles as the subjects flexed or extended their fingers. The EMG signals were amplified and sampled using the EMG-USB2+ system (OT Bioelettronica) with a gain of 1000, a passband of 10–900 Hz, and a sampling rate of 2048 Hz. The reference electrode was placed at the wrist.

To measure the flexion forces of the index, middle, and ring fingers, we used three miniature load cells (SM-200N, Interface) with a sampling frequency of 1000 Hz, as shown in Fig. 1. During the data acquisition, the forearm was supported in a neutral position, and the wrist was stabilized with two stiff foam pads to minimize force transmission from the wrist and other proximal joints.

3) Experiment Procedure: Before the main experiment, we measured the maximum voluntary contraction (MVC) finger flexion force. During the experiment, subjects tracked a predefined force target with a pseudorandom pattern, in the range of 0%–50% MVC for each finger. We selected this force

level because it covered the level of muscle activation in a majority of the daily tasks while avoiding muscle fatigue.

Each subject performed two types of finger flexion trials: single-finger trials and multifinger trials. In the single-finger trials, only one finger followed the trapezoidal force pattern, and the participants were instructed to avoid co-contraction of other fingers. Subjects performed three repetitions of the single-finger trials for the index, middle, and ring fingers. In the multifinger trials, the index, middle, and ring fingers were flexed simultaneously, comprising three multifinger trials. Thus, each session included a total of nine single-finger trials and three multifinger trials.

To assess the performance of neural-drive-based force prediction cross sessions, three sessions were conducted for each subject at varied time intervals (6.58 $\pm$ 6.47 days), depending on the availability of the subjects.

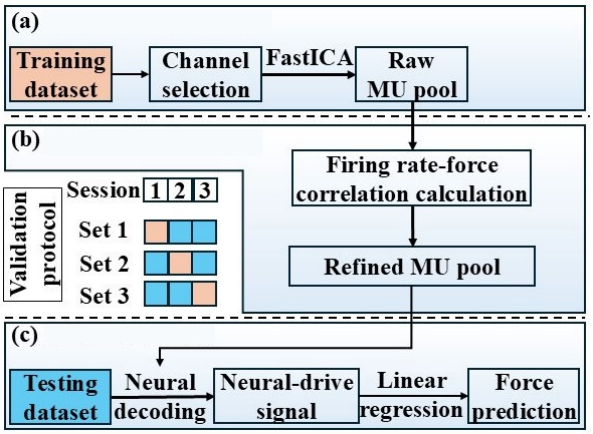

Fig. 2. Cross-session flowchart of the neural-decoding algorithm. (a) Initial MU extraction. (b) MU pool refinement. (c) Force prediction.

B. Signal Preprocessing

To reduce noise, the EMG signals were initially filtered using a fourth-order high-pass Butterworth filter with a cutoff frequency of 20 Hz. Subsequently, motion artifacts were eliminated using our previously established method [28].

C. Force Prediction Based on Neural Drive

1) Initial MU Extraction: The EMG signals of the single-finger trials were used to form the preliminary MU pool. We first selected the 60 most active channels with the highest root-mean-square (rms) value out of the 128-channel EMG signals for the extensor and flexor of each finger to reduce computational load. The number of channels was determined based on our previous work [29]. For each session, the rms of each channel was calculated for every single-finger trial. The results for the same finger trials were averaged, and the top active 60 channels were identical cross sessions, which was necessary for cross-session evaluations.

Motoneuron firing activities were obtained by decomposing the 60-channel EMG signals using a previously developed FastICA algorithm [30]. Detailed steps are provided in the supplementary material. Briefly, we first extended the EMG signals to increase the number of observations and whitened the extended signals to remove the correlation between observations. Then, we performed FastICA to decompose the signals and obtained the separation vectors and source signals for individual MUs. Each separation vector represented an MU, and the corresponding source signal reflected the spike train of the MU. For binary classification, the source signals were then transformed into a discharge event train using the K-means^{++} clustering algorithm [31]. We removed low-quality MUs. The silhouette distance of the cluster was then computed, and separation vectors with a silhouette value below 0.5 were considered to be inaccurate. The inaccurate MUs were eliminated. This process yielded the initial separation matrices for individual fingers.

2) MU Pool Refinement: Due to the co-activation of finger muscles, it is challenging to keep other fingers completely inactive when flexing a specific finger. As a result, some MUs in the separation matrix may correspond to MUs of other fingers. To address this problem, a refinement process was applied to identify and exclude MUs not associated with the target finger. This was done by comparing a correlation between the discharge activity of each MU and the force signals from the three fingers. MUs corresponding to other fingers were removed, ensuring that the refined separation matrix accurately reflected the target finger muscle activity.

Specifically, the initial separation matrix for finger i (index, middle, or ring finger) was used to decompose every single-finger trial, and we then obtained the firing rates of each MU. For each MU in the MU pool, a linear regression was performed between the firing rates and the force signals, and we calculated the R^2 value of the regression. If the R^2 value obtained from trials of other fingers was higher than that from finger i, it was considered that the MU did not belong to finger i, and the associated separation vector was removed from the separation matrix of finger i, thereby giving us the refined separation matrices specific to individual fingers.

3) Force Prediction: The refined separation matrix was used to decompose the EMG signals, producing spike trains for each MU in the MU pool. The spike trains from all MUs were then summed to represent the populational firing rate, which was the neural drive for finger force predictions.

The data were divided into training (one session) and testing sets (two other sessions) to evaluate the force prediction performance (Fig. 2). We multiplied the refined separate matrices to the testing EMG data. The firing rate of each MU was calculated. A moving window of 500 ms with a step size of 125 ms was used for the populational firing rate calculation. The populational firing rate of each window was computed as the sum of spike trains from all retained MUs in the window. A Kalman filter was applied to the populational firing rate to smooth the populational firing rate signals, using a system matrix of 1, an observation matrix of 1, a system covariance of 0.1, and an observation covariance of 0.5. The corresponding force signals were also smoothed using the same window.

To predict the forces of finger i, the populational firing rates of the extensor and flexor were used, due to potential co-activations of the muscle pairs. Specifically, a linear regression was performed between the populational firing rates and force signals of the training dataset

$$F_i(t) = aD_{i,\text{ext}}(t) + bD_{i,\text{flx}}(t) + c \quad (1)$$

where $F_i(t)$ is the predicted force of finger i (i = index, middle, or ring) over time t; $D_{i,\text{ext}}(t)$ is the extensor populational firing rate of finger i; $D_{i,\text{flx}}(t)$ is the flexor populational firing rate of finger i; and a, b, and c are the coefficients of the linear regression.

The performance of the neural-drive-based force prediction was then evaluated using the testing dataset. The prediction performance was assessed by comparing the predicted force with the actual force by calculating the coefficient of determination (R^2) and RMSE.

4) Complexity Analysis: The computational complexity for each 500-ms EMG segment during the testing process is $O(k \cdot N \cdot m)$, where k is the column dimension of the refined separation matrix, which corresponds to the number of MUs in the refined MU pool derived from the training data; N is the number of the extended EMG channels; and m is the number of data points in each segment. In this study, $k = 41.51 \pm 15.71$, $N = 600$, and $m = 1024$.

D. Force Prediction Based on EMG-Amplitude

The force prediction based on conventional EMG amplitude was also implemented for comparison.

1) EMG-Amplitude Calculation: We used the top 60 most active channels for the EMG-amplitude-based force prediction, and the same channel set is used for EMG decomposition in the neural-drive method. The EMG amplitude was quantified using rms values using the same windowing procedure as the neural-drive method (a moving window of 500 ms with a step size of 125 ms). The EMG amplitude of each window was calculated as the average rms of the 60 channels of that window.

2) Force Prediction: The same Kalman filter was applied to smooth the rms values. The corresponding force signals were also smoothed using the same windowing and filtering parameters. A linear regression was performed between the EMG amplitude and force signals in the training set, as described in the following equation:

$$F_i(t) = aA_{i,\text{ext}}(t) + bA_{i,\text{flx}}(t) + c \tag{2}$$

where $F_i(t)$ is the predicted force of finger i (i = index, middle, or ring); $A_{i,\text{ext}}(t)$ is the extensor EMG amplitude of finger i, $A_{i,\text{flx}}(t)$ is the flexor EMG amplitude of finger i; and a, b, and c are the coefficients of the linear regression.

3) Complexity Analysis: The computational complexity for each 500-ms segment during the testing process is $O(n \cdot m)$, where n is the number of EMG channels and m is the number of data points in each segment. In this study, $n = 60$ and $m = 1024$.

E. Evaluation Protocols

We evaluated the performance of force prediction cross sessions and within session. Two assignment protocols, Protocols 1 and 2, were applied for the assignment of the training and testing sets. Specifically, for the force prediction on finger i, the testing set of both protocols included single-finger trials of finger i and multifinger trials. Protocol 1 included both single-finger and multifinger trials in the training set, while Protocol 2 only included single-finger trials. These two protocols aimed to evaluate the robustness of the force prediction model when trained on a comprehensive dataset of a variety of tasks or a specific dataset of a single task.

1) Cross-Session Validation Protocol: For each subject, the training and testing sets came from different sessions. The data from each session was utilized as the training data, and the data from the other two sessions served as the testing dataset (Fig. 2). In Protocol 1, all the single-finger and multifinger trials of finger i served as the training dataset. In Protocol 2, only the single-finger trials of finger i were employed as the training dataset. The testing dataset included both the single-finger trials and multifinger trials from the testing sessions.

2) Within-Session Validation Protocol: We also performed force prediction within a session to compare with the cross-session predictions. Both the training and testing datasets were derived from the same session. For each finger, there were three single-finger trials and three multifinger trials in a session. In Protocol 1, one out of the six trials served as the testing dataset, and the remaining five trials formed the training set. In Protocol 2, the testing dataset was the same as Protocol 1, but only the single-finger trials of the training dataset in Protocol 1 were used for training.

F. Statistical Analysis

The accuracy of force prediction based on the neural drive and EMG amplitude was evaluated using the RMSE and R^2 values. The RMSE and R^2 values were analyzed using the Friedman test and Wilcoxon signed-rank test because the data did not follow a normal distribution. The significance level was set to 0.05. The Holm–Bonferroni correction was applied to avoid multiple-comparison errors.

III. Results

A. Variability of EMG Signals Across Sessions

Fig. 3 presents the examples of the EMG-amplitude (rms) distribution for single-finger trials cross sessions for the index [Fig. 3(a)], middle [Fig. 3(b)], and ring [Fig. 3(c)] fingers. Both the extensor and flexor muscles were presented. The red point in each heatmap showed the peak EMG amplitudes. Although the activation patterns for the same tasks were generally consistent cross sessions, there were notable differences in the location of the overall activation area. We quantified the degree of similarity of the activation pattern using a 2-D cross correlation between the same type of heatmaps cross sessions. The average correlation coefficients of the heatmaps cross session were 0.69 for the index finger, 0.74 for the middle finger, and 0.75 for the ring finger. The Friedman test demonstrated there were no significant differences among the correlation coefficients between different sessions for the index ($\chi 2(2) = 2.62$ and $p = 0.2691$), middle ($\chi 2(2) = 2.62$ and $p = 0.2691$), and ring fingers ($\chi 2(3) = 1.62$ and $p = 0.4437$).

B. Representative Results of Force Prediction

Fig. 4 shows the representative predicted forces of the index finger using the two methods. Due to the similarity among

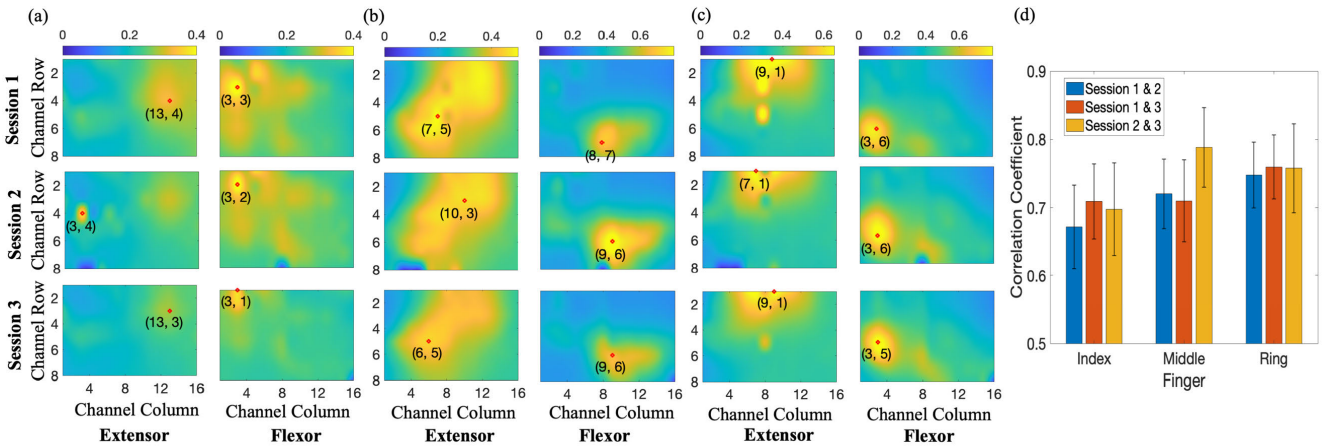

Fig. 3. Distribution of EMG amplitude (rms) when flexing (a) index, (b) middle, and (c) ring fingers in three different sessions. The red points are the peak positions of the EMG amplitudes. (d) Two-dimensional correlation coefficient (average ± standard error) between heatmaps cross sessions for the index, middle, and ring fingers.

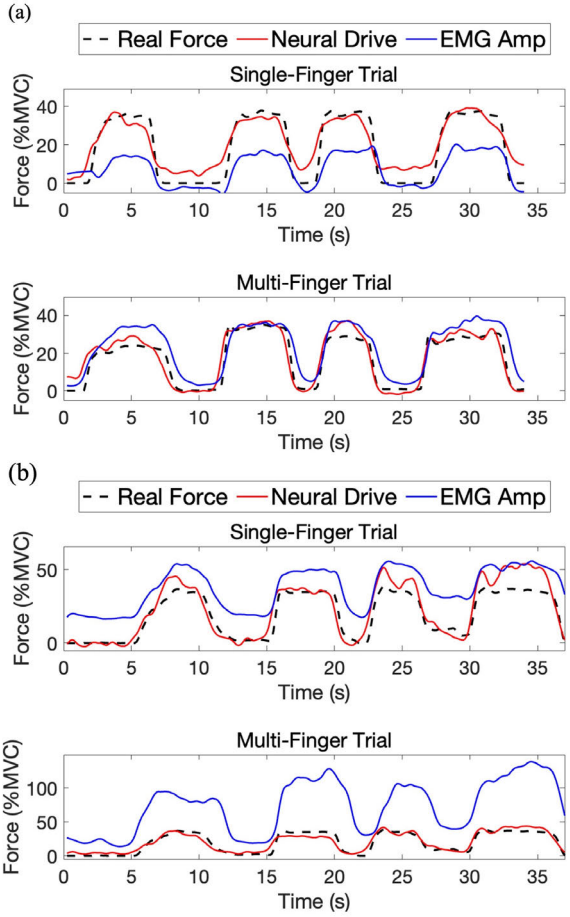

Fig. 4. Exemplar results of index finger force predictions of a single trial based on neural-drive method and EMG-amplitude method obtained in (a) within-session mode with Protocol 1 and (b) cross-session mode with Protocol 2.

the results of the within-session mode with Protocols 1 and 2 and the cross-session mode of Protocol 1, only the results of the within-session mode of Protocol 1 were presented here. Compared with the results of the EMG-amplitude method, the predictions of the neural-drive method exhibited higher accuracy values. In most training schemes and modes, the forces predicted by the EMG-amplitude method deviated considerably from the ground truth. However, the forces predicted using the neural-drive method closely matched the actual force values. This indicated that the neural-drive-based force prediction had a better performance than the EMG-amplitude-based force prediction.

C. Performance of Force Prediction Based on Neural Drive

Fig. 5 summarizes the performance of neural-drive-based force prediction measured by RMSE across sessions [Fig. 5(a)] and within a session [Fig. 5(b)]. The results of the correlation of determination (R^2) exhibited a consistent trend with the RMSE; therefore, only the RMSE results were presented here. The average RMSE of the cross-session mode was 8.28% MVC, while the average RMSE of the within-session mode was 6.43% MVC. The Wilcoxon signed-rank test showed a significant difference between the force prediction performance of the two modes ($p = 0.0004$).

For force predictions across sessions, the Friedman test demonstrated significant differences among the different training schemes for the index finger ($\chi^2(3) = 12.15$ and $p = 0.0069$), the middle finger ($\chi^2(3) = 21.75$ and $p = 0.0001$), and the ring finger ($\chi^2(3) = 11.85$ and $p = 0.0079$). For force predictions of all three fingers, "Protocol 1 single-finger trials" demonstrated the best performance (index: (6.25% ± 0.15%) MVC, middle: (6.52% ± 0.16%) MVC, and ring: (7.37% ± 0.24%) MVC). In contrast, the worst performance was observed in "Protocol 2 multifinger trials" (index: (10.97% ± 0.38%) MVC, middle: (9.46% ± 0.32%) MVC, and ring: (12.08% ± 0.45%) MVC). The differences in average RMSE between the best and worst protocols were 4.72% MVC ($p = 0.0156$) for the index finger, 2.94% MVC ($p = 0.0078$) for the middle finger, and 4.71% MVC ($p = 0.0156$) for the ring finger.

For force prediction within sessions, there were still significant differences among the various training schemes for the index finger ($\chi 2(3) = 14.55$ and $p = 0.0022$), middle finger ($\chi 2(3) = 19.95$ and $p = 0.0002$), and ring finger ($\chi 2(3) = 18.60$ and $p = 0.0003$). The force predictions for all three fingers were consistent. The best performances were observed in "Protocol 2 single-finger trials," with results of (5.21% ± 0.29%) MVC for the index finger, (5.13% ± 0.18%) MVC for the middle

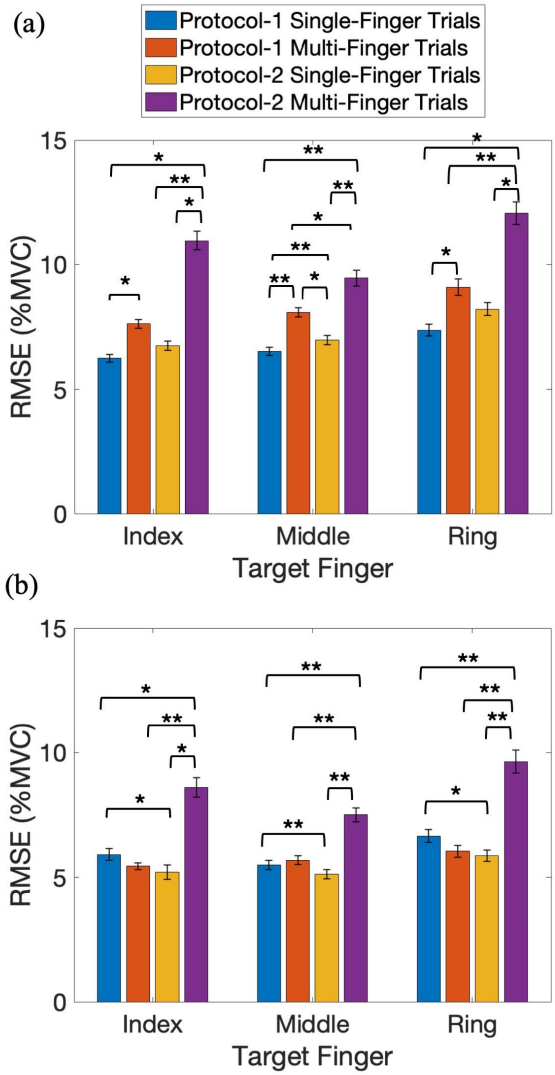

Fig. 5. Performance (RMSE average ± standard error) of neural-drive-based force prediction with different training protocols for single-finger trials and multifinger trials of the index, middle, and ring fingers across sessions (a) and within a session (b). *: $p < 0.05$. **: $p < 0.01$.

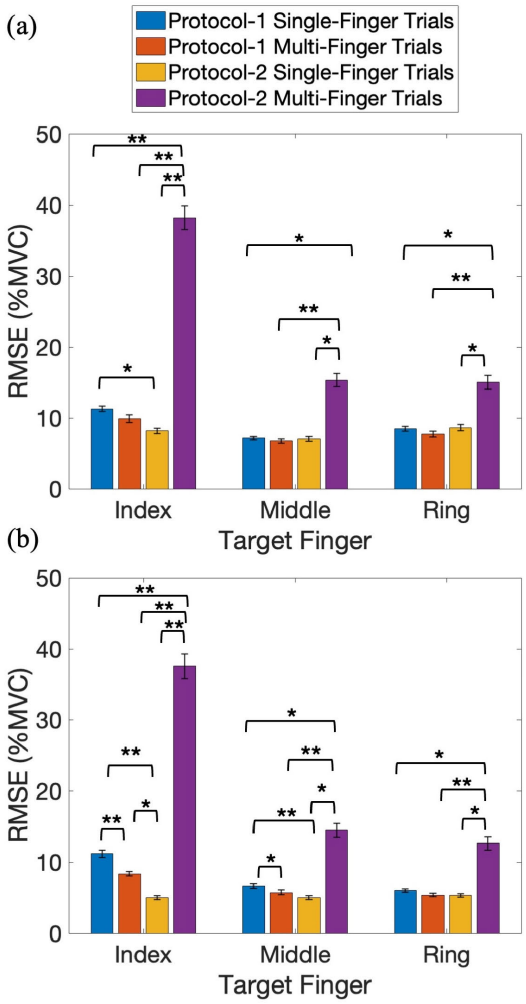

Fig. 6. Performance (RMSE average ± standard error) of EMG-amplitude-based force predictions with different training protocols for the single-finger trials and multifinger trials of (a) index, middle, and ring fingers across sessions and (b) within a session. *: $p < 0.05$. **: $p < 0.01$.

finger, and (5.87% ± 0.22%) MVC for the ring finger. Conversely, the worst performances occurred in "Protocol 2 multifinger trials," with (8.60% ± 0.39%) MVC for the index finger, (7.50% ± 0.28%) MVC for the middle finger, and (9.63% ± 0.46%) MVC for the ring finger. The average RMSE differences between the best and worst protocols were 3.39% MVC ($p = 0.0156$) for the index finger, 2.37% MVC ($p = 0.0078$) for the middle finger, and 3.76% MVC ($p = 0.0078$) for the ring finger.

In summary, the neural-drive-based force prediction algorithm demonstrated a robust performance across various conditions. It maintained high accuracy and consistency across sessions and within a session, adapted well to different types of motor tasks, and performed reliably for different fingers.

D. Performance of Force Prediction Based on EMG-Amplitude

Fig. 6 summarizes the performance of EMG-amplitude-based force prediction measured by RMSE across sessions [Fig. 6(a)] and within a session [Fig. 6(b)]. The trend observed in the R^2 results mirrored that of the RMSE; thus, we only presented the RMSE results. Training schemes impacted the prediction accuracy for EMG-amplitude-based force prediction. The average RMSE for the cross-session mode was 11.96% MVC, while the average RMSE for the within-session mode was 10.28% MVC. The Wilcoxon signed-rank test showed a significant difference between force prediction performance in the two modes ($p = 0.0005$).

Across sessions, significant differences were found among the various training schemes for the index finger ($\chi^2(3) = 17.55$ and $p = 0.0005$), middle finger ($\chi^2(3) = 12.45$ and $p = 0.0060$), and ring finger ($\chi^2(3) = 12.30$ and $p = 0.0064$). For the index finger, the best performance was observed in "Protocol 2 single-finger trials" [(8.17% ± 0.36%) MVC]. For middle and ring fingers, the best performances were observed in "Protocol 1 multifinger trials" (middle: (6.72% ± 0.32%) MVC and ring: (7.73% ± 0.42%) MVC). The worst performances for the three fingers occurred in "Protocol 2 multifinger trials" (index: (38.21% ± 1.65%) MVC, middle: (15.32% ± 0.93%) MVC, and ring: (15.04% ± 0.95%) MVC). The difference in average RMSE between the best and worst protocols was

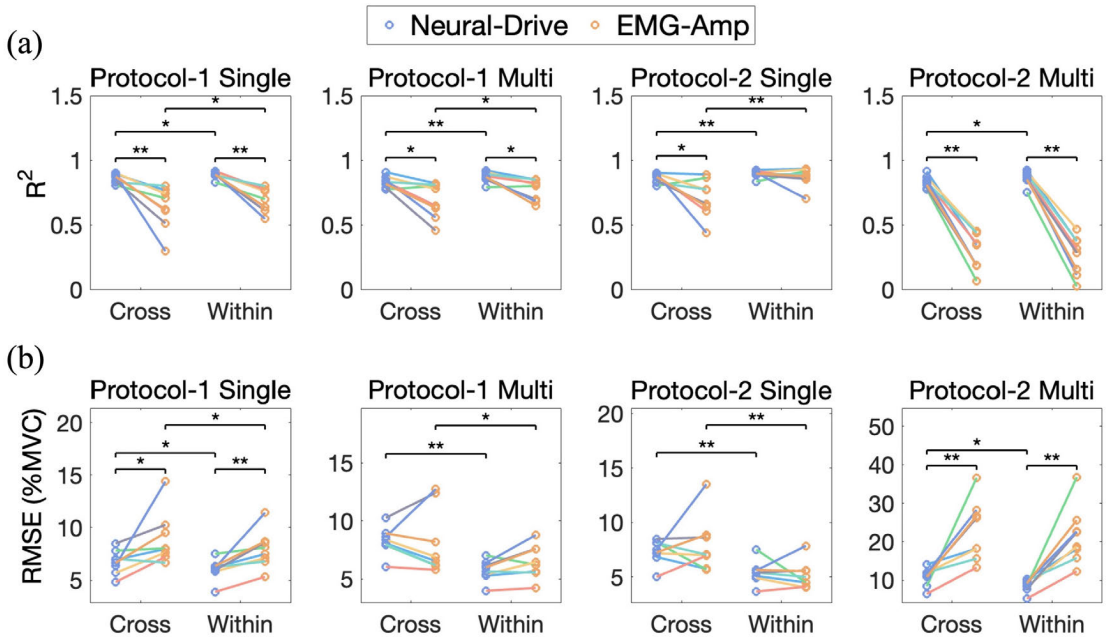

Fig. 7. (a) R^2 and (b) RMSE obtained with different training schemes of the neural drive and EMG amplitude. Each symbol represents an individual subject. *: $p < 0.05$. **: $p < 0.01$.

30.04% MVC ($p = 0.0078$) for the index finger, 8.60% MVC ($p = 0.0078$) for the middle finger, and 7.31% MVC ($p = 0.0078$) for the ring finger.

Within sessions, there were significant differences among different training schemes as well for the index finger ($\chi^2(3) = 22.95$ and $p = 0.0000$), middle finger ($\chi^2(3) = 14.85$ and $p = 0.0019$), and ring finger ($\chi^2(3) = 13.35$ and $p = 0.0039$) based on the Friedman test. The force predictions for all three fingers were consistent. The best performances occurred in "Protocol 2 single-finger trials," with results of (5.04% ± 0.25%) MVC for the index finger, (5.03% ± 0.30%) MVC for the middle finger, and (5.34% ± 0.26%) MVC for the ring finger. Conversely, the worst performances occurred in "Protocol 2 multifinger trials," with (37.53% ± 1.77%) MVC for the index finger, (14.46% ± 0.99%) MVC for the middle finger, and (12.62% ± 0.91%) MVC for the ring finger. The average RMSE differences between the best and worst protocols were 32.49% MVC ($p = 0.0078$) for the index finger, 9.43% MVC ($p = 0.0156$) for the middle finger, and 7.28% MVC ($p = 0.0156$) for the ring finger.

In summary, the performance of force prediction of the EMG-amplitude approach heavily depended on the training protocol. The method showed low robustness when the training scheme and types of tasks changed.

E. Comparison of the Neural-Drive Method and EMG-Amplitude Method

We then compared the performance of the two different methods in different settings. Fig. 7 illustrates the summary results of different force prediction methods. The performances were quantified by the correlation of determination (R^2) and RMSE. Fig. 7(a) presents the R^2 values for each task. In most cases, R^2 of force prediction based on the neural-drive method was higher than that based on the EMG-amplitude method ($p < 0.05$), indicating that the neural-drive method more accurately utilized MU information to predict forces. As shown in Fig. 7(b), the RMSE obtained using the neural-drive method was lower than that of the EMG-amplitude method ($p < 0.05$). In addition, the RMSE for the eight subjects was more consistent when using the neural-drive method, indicating that this method consistently predicted forces accurately across subjects. This demonstrated the superior performance and robustness of the neural-drive method.

TABLE I

FRIEDMAN TEST RESULTS FOR R^2 AND RMSE AMONG FOUR COMPARISON GROUPS (NEURAL DRIVE/EMG AMPLITUDE AND CROSS SESSION/WITHIN SESSION) IN EACH TRAINING SCHEMES (*: $p < 0.05$ AND **: $p < 0.01$)

Training Scheme		R^2		RMSE	
		χ^2 (3)	p-value	χ^2 (3)	p-value
Protocol-1	Single	21.15	0.0001	17.70	0.0005
	Multi	13.95	0.0030	14.55	0.0022
Protocol-2	Single	14.85	0.0019	14.85	0.0019
	Multi	20.70	0.0001	20.70	0.0001

According to Table I, for the four different training schemes, significant differences were observed among the different training models according to the Friedman test in both R^2 and RMSE. According to the Wilcoxon signed-rank test, in all the cases except Protocol 2 of single-finger trials in the within-session mode, there were significant differences between the R^2 obtained by the neural-drive method and the EMG-amplitude method (Table II). According to Table III, for the neural-drive method, there were significant differences between the performance in cross-session mode and within-session mode in both R^2 and RMSE. For EMG amplitude with all the training schemes except for using Protocol 2 to test the multifinger trials, there were significant differences between cross-session mode and within-session mode in both R^2 and RMSE. However, for the "Protocol-2 multifinger trials," both cross-session and within-session force prediction based on the EMG-amplitude method performed significantly worse than those based on the neural-drive method.

TABLE II

WILCOXON SIGNED-RANK TEST RESULTS (p-VALUE) FOR R^2 AND RMSE BETWEEN NEURAL-DRIVE METHOD AND EMG-AMPLITUDE METHOD (*: $p < 0.05$ AND **: $p < 0.01$)

Training Scheme		Task	R^2	RMSE
Protocol-1	Single	Cross	0.0078	0.0234
		Within	0.0078	0.0078
	Multi	Cross	0.0234	0.7422
		Within	0.0156	0.0781
Protocol-2	Single	Cross	0.0391	0.8438
		Within	0.5469	0.5469
	Multi	Cross	0.0078	0.0078
		Within	0.0078	0.0078

TABLE III

WILCOXON SIGNED-RANK TEST RESULTS (p-VALUE) FOR R^2 AND RMSE BETWEEN CROSS-SESSION AND WITHIN-SESSION TASKS (*: $p < 0.05$ AND **: $p < 0.01$)

Training Scheme		Neural-Drive		EMG-Amplitude	
		R^2	RMSE	R^2	RMSE
Protocol-1	Single	0.0156	0.0156	0.0391	0.0391
	Multi	0.0078	0.0078	0.0156	0.0156
Protocol-2	Single	0.0078	0.0078	0.0078	0.0078
	Multi	0.0234	0.0156	0.4609	0.2500

The testing process of each 500-ms EMG segment using the neural-drive method required an average of 55.43 ms and 9.67 MB of memory, whereas the EMG-amplitude method required an average of 0.83 μs and 18.30 bytes of memory.

In summary, the neural-drive method outperformed the EMG-amplitude method in force prediction based on EMG signals, demonstrating superior accuracy and robustness. In most cases, the force prediction performance within a session was better than that cross sessions. However, the high decoder accuracy is associated with the cost of high computational complexity.

IV. DISCUSSION

In this study, we developed a robust neural-decoding approach feasible for multiday motor intent predictions. We evaluated the decoder performance for within-session and cross-session finger force predictions, to demonstrate the viability of this approach for practical use. Our results revealed that our method could achieve comparable results to previous research [27], [29] in within-session force predictions, and more importantly, we found that our decoder maintained stable performance in cross-session conditions. Specifically, we obtained EMG data across three sessions following the same procedures, decomposed the data from one session using the FastICA algorithm, and refined the MU pool for accurate finger force predictions. We then applied the refined separation matrix to the EMG signals of the other two sessions to obtain cross-session neural-drive signals in a real-time manner, which were mapped to individual finger forces using a regression function. Compared with the EMG-amplitude approach, our neural-drive method consistently achieved high cross-session prediction performance, demonstrating robustness and reliability for long-term neural-machine interaction without the need for frequency recalibrations.

A. Comparison With Previous Studies

Previous studies have aimed to improve the accuracy and robustness of EMG-based finger force prediction. The majority of studies focused on finger force predictions within a single recording session. For example, an earlier study [32] performed force prediction based on EMG amplitude (root mean square) by exploring different channel merging and selection approaches. Their models achieved average RMSE values around 6%–10% MVC. Our models achieved an average RMSE of around 5%–10% MVC, and the best-performance protocol achieved an average RMSE of 5.40% MVC. A previous work [33] combined accelerometry signals with EMG features for finger force prediction. Their model achieved an average R^2 of 0.93 with the optimal feature set. Our neural-drive method was based on EMG alone and achieved an average R^2 of 0.90 with the optimal protocol. An earlier work [34] also employed the neural-drive method to predict multifinger forces within a session. They constructed the MU pool using data from single-finger trials along with a subset of multifinger trials and then applied this MU pool to predict forces in multifinger trials, achieving an average R^2 of 0.72. In our approach, the MU pool was only constructed using single-finger trials, and the average R^2 values for multifinger trials were 0.87 (Protocol 1) and 0.86 (Protocol 2). In the within-session mode, our neural-drive-based finger force prediction approach achieved performance comparable to that of previous studies. However, research on cross-session finger force prediction remains scarce. An earlier study [35] demonstrated the consistency of MU spike trains across sessions using elbow flexion EMG data from a single subject, providing preliminary evidence for the feasibility of applying the neural-drive-based approach to cross-session force predictions. Building on this foundation, our study further validated the superiority of the neural-drive approach in cross-session force predictions through individual finger force estimation tasks.

In earlier studies [27], [29], [36], we applied the neural-drive-based approach to both dynamic joint angle estimation and isometric force estimation within sessions. We tested various conditions, including flexion and extension movements for each finger, single-finger and multifinger trials, and different electrode placements. These previous results support the effectiveness of the approach in achieving continuous and reliable joint kinematic predictions. In the current study, we extended the neural-drive method to cross-session force predictions, and we implemented two protocols to assess the robustness of the approach across four different cases. The results show that the neural-drive approach significantly enhances the long-term reliability of finger force predictions and holds promise for a wide range of practical applications. Therefore, these studies together provide valuable insights into the efficacy and performance of the neural-drive approach for predicting finger kinematic features.

B. Comparison of EMG-Amplitude and Neural-Drive Approaches for Force Prediction

For the EMG-amplitude approach, the force prediction performed better in the within-session evaluation compared

with the cross-session evaluation. This was because EMG signals were easily affected by the following factors. First, the electrode position could have shifted between sessions due to inconsistent electrode reattachment, which can be indicated by the shift of activation areas across sessions in Fig. 3. Correspondingly, the electrode shifts can potentially lead to different overall EMG amplitude over sessions. Second, changes in the muscle physiological properties due to exercise history or hydration levels over time could contribute to the variations of EMG amplitude observed between sessions. Third, background noise differences across sessions may also lead to varying SNRs, further affecting the cross-session force prediction performance. Finally, the outlier electrode channels may be different across sessions due to variations in skin-electrode contact impedance. The variation in inactive EMG channels could affect the reliability of the EMG-amplitude force estimation.

In contrast, the neural-decoding approach was relatively robust over sessions, which can be attributed to the nature of the binary motoneuron discharge events. Specifically, the neural-drive signals for the finger force prediction rely on the binary motoneuron discharge events decomposed from EMG signals. The binary representation mainly focuses on the timing of neural events, which tends to be more consistent despite variations in their amplitude or waveform characteristics. In addition, the EMG signal variations are less likely to affect the decoded neural-drive signals. This is because the binary encoding does not rely on these properties but rather on the detection of the occurrence of action potentials, thereby maintaining consistency across different sessions. Moreover, the EMG decomposition procedure can effectively remove background noise and motion artifacts. The primary objective of the FastICA algorithm is to identify and separate statistically independent source components, which isolates actual muscle activity from various noise sources by maximizing the non-Gaussianity of the components. When we exclude source signals with low silhouette values, those poorly separated sources can be removed [37]. It is worth noting that it was unexpected that the earlier derived separation matrices can still reliably function on the new dataset despite variations in the EMG signals. As shown in our earlier work [38], the decomposition accuracy did decline after sustained muscle activations. We believe that the nature of the neural-drive calculation can tolerate inaccurate spike detections. Namely, the populational MU firing rate averages the mean firing rate of multiple MUs in a large window (e.g., 0.5 s), and any small spike timing errors (considered low decomposition accuracy) would not be reflected in the overall average firing rate profile.

Similar to the cross-session performance, the neural-drive approach outperformed the EMG-amplitude approach in the within-session force prediction performance. In addition to the discussed factor of surrounding noise, the enhanced performance can be primarily attributed to the effective process of crosstalk among finger muscle compartments using the neural-drive approach. Specifically, the spatial proximity of finger muscle compartments often leads to signal crosstalk, which consequently results in biased force predictions due to either overestimation or underestimation of the muscular activities using the EMG-amplitude approach. Although the influence of crosstalk can be reduced by the channel selection procedure, this interference may still be present in the remaining channels [34]. As a comparison, the neural-drive approach classified MUs specific to individual fingers. With those specific MUs, we can ensure independent prediction of neural-drive signals for each finger despite closely related anatomical structures between finger muscle compartments.

C. Comparison of Protocols for Single-Finger and Multifinger Force Prediction

We systematically investigated the finger force prediction performance under two protocols. As shown in Fig. 7, the overall prediction performance of single-finger trials under Protocol 2 was superior to that observed under Protocol 1, indicating that Protocol 2 was more effective in scenarios involving isolated finger movements. However, this advantage did not extend to multifinger tasks, where the prediction performance for multifinger force tasks deteriorated under Protocol 2. The primary reason for this discrepancy lies in the differences in the training schemes employed by the two protocols. Under Protocol 2, the models were exclusively trained using single-finger data. Although this approach optimized the models for single-finger tasks, it inadvertently led to overfitting. Consequently, the models became highly specialized for single-finger predictions but exhibited poor generalization when applied to multifinger trials. In contrast, Protocol 1 adopted a more comprehensive training scheme. The models were trained using a combination of both single-finger and multifinger data. This inclusive approach enabled a more balanced prediction capability, ensuring that the models could perform well across both types of tasks. The model training procedure under Protocol 1 minimized the risk of overfitting to single-finger data, thereby enhancing the generalization ability of the models.

D. Limitations

Although we have achieved promising cross-session results with our developed neural-drive approach, it has several limitations. For example, we only considered isometric finger force. In future studies, we plan to validate our neural-drive approach for the prediction of finger kinematics during movements. In addition, our focus was limited to the three fingers, excluding the picky finger and thumb. The picky finger was not included because of substantial co-activation between the picky and the ring fingers, which was difficult to separately predict the forces of each finger. The thumb was excluded due to its unique anatomy and movements which our forearm EMG data cannot accurately capture. Future efforts could expand data collection to include EMG signals from the intrinsic muscles of the thumb, thereby enhancing the validation of our neural-decoding approach for thumb force prediction. In addition, while the neural-drive method demonstrated accurate and robust long-term finger force predictions, it is associated with high computational time and memory utility. However, the computational time (approximately 55 ms) is well within

the real-time decoding constraint of below 100 ms for real-time implementations. Finally, we did not address the effect of muscle fatigue, which could impact the reliability of MU decomposition due to drift of action potential waveforms. In future studies, we plan to assess the performance of the neural-drive approach under these challenging conditions.

V. Conclusion

In this study, we evaluated the long-term stability of finger force predictions using our developed neural-drive approach. Our neural-drive approach can outperform the EMG-amplitude approach for both within-session and cross-session evaluation protocols. In addition, we observed less amount of cross-session performance degradation using our developed approach than that using the EMG-amplitude approach. The outcomes offer a reliable neural-decoding approach across sessions. The robustness of our approach was clearly demonstrated across various conditions, proving its potential for practical applications where long-term reliability is critical.

References

[1] S. Kadalagere Sampath, N. Wang, H. Wu, and C. Yang, "Review on human-like robot manipulation using dexterous hands," *Cogn. Comput. Syst.*, vol. 5, no. 1, pp. 14–29, Mar. 2023.

[2] J. Lai et al., "A novel soft glove utilizing honeycomb pneumatic actuators (HPAs) for assisting activities of daily living," *IEEE Trans. Neural Syst. Rehabil. Eng.*, vol. 31, pp. 3223–3233, 2023.

[3] E. Drelich et al., "Force prediction in the cylindrical grip for a model of hand prosthesis," *Sci. Rep.*, vol. 13, no. 1, p. 17205, Oct. 2023.

[4] Q. Xie et al., "Design of a SMA-based soft composite structure for wearable rehabilitation gloves," *Frontiers Neurorobotics*, vol. 17, pp. 1–18, Feb. 2023, Art. no. 1047493.

[5] L. Zongxing et al., "Human–Machine interaction technology for simultaneous gesture recognition and force assessment: A review," *IEEE Sensors J.*, vol. 23, no. 22, pp. 26981–26996, Nov. 2023.

[6] J. Jiang, Z. Gao, and G. Li, "A miniature elastic torque sensor for index finger exoskeletons," *IEEE Trans. Instrum. Meas.*, vol. 72, pp. 1–10, 2023.

[7] B. G. Dutra and A. D. S. Silveira, "Multivariable grasping force control of myoelectric multi-fingered hand prosthesis," *Int. J. Dyn. Control*, vol. 11, no. 6, pp. 3145–3158, Mar. 2023.

[8] G. Li et al., "Multicontact intrinsic force sensing method of a flexible finger for hand assistance," *IEEE Trans. Instrum. Meas.*, vol. 73, pp. 1–12, 2024.

[9] M. M. Keller, R. Y. Barnes, and C. Brandt, "Activities of daily living with grasp types and force measurements during object manipulation," *South Afr. J. Occupational Therapy*, vol. 54, no. 1, pp. 15–21, Apr. 2024. [Online]. Available: https://orcid.org/0000-0002-8445-1348

[10] R. A. Romeo et al., "Instrumenting a robotic finger to augment the capabilities of robotic grippers," *IEEE Trans. Instrum. Meas.*, vol. 72, pp. 1–11, 2023.

[11] Y. Yan et al., "Grasping-Force-Based passive safety method for a vascular interventional surgery robot system," *IEEE Trans. Instrum. Meas.*, vol. 72, pp. 1–12, 2023.

[12] C. Lyu et al., "Deep-Learning-Based force sensing method for a flexible endovascular surgery robot," *IEEE Trans. Instrum. Meas.*, vol. 73, pp. 1–10, 2024.

[13] O. Postolache, D. J. Hemanth, R. Alexandre, D. Gupta, O. Geman, and A. Khanna, "Remote monitoring of physical rehabilitation of stroke patients using IoT and virtual reality," *IEEE J. Sel. Areas Commun.*, vol. 39, no. 2, pp. 562–573, Feb. 2021.

[14] C. Y. Neng and M. K. Ishak, "Internet of Things (IoT) based flex force smart glove for physical rehabilitation," in *Proc. IEEE-EMBS Conf. Biomed. Eng. Sci. (IECBES)*, Langkawi Island, Malaysia, Mar. 2021, pp. 276–280.

[15] T. Lenzi, S. M. M. De Rossi, N. Vitiello, and M. C. Carrozza, "Intention-based EMG control for powered exoskeletons," *IEEE Trans. Biomed. Eng.*, vol. 59, no. 8, pp. 2180–2190, Aug. 2012.

[16] B. Farrokhi and A. Erfanian, "A state-based probabilistic method for decoding hand position during movement from ECoG signals in non-human primate," *J. Neural Eng.*, vol. 17, no. 2, May 2020, Art. no. 026042.

[17] S. M. Hosseini and V. Shalchyan, "State-based decoding of continuous hand movements using EEG signals," *IEEE Access*, vol. 11, pp. 42764–42778, 2023.

[18] A. Ahmadi, A. Khorasani, V. Shalchyan, and M. R. Daliri, "State-based decoding of force signals from multi-channel local field potentials," *IEEE Access*, vol. 8, pp. 159089–159099, 2020.

[19] L. Meng et al., "User-tailored hand gesture recognition system for wearable prosthesis and armband based on surface electromyogram," *IEEE Trans. Instrum. Meas.*, vol. 71, pp. 1–16, 2022.

[20] Y. Na, C. Choi, H.-D. Lee, and J. Kim, "A study on estimation of joint force through isometric index finger abduction with the help of SEMG peaks for biomedical applications," *IEEE Trans. Cybern.*, vol. 46, no. 1, pp. 2–8, Jan. 2016.

[21] Z. Wang et al., "Optimization of inter-subject sEMG-based hand gesture recognition tasks using unsupervised domain adaptation techniques," *Biomed. Signal Process. Control*, vol. 92, Jun. 2024, Art. no. 106086.

[22] J. Fan, X. Jiang, X. Liu, L. Meng, F. Jia, and C. Dai, "Surface EMG feature disentanglement for robust pattern recognition," *Expert Syst. Appl.*, vol. 237, Mar. 2024, Art. no. 121224.

[23] Y. Guo et al., "SEMG-based inter-session hand gesture recognition via domain adaptation with locality preserving and maximum margin," *Int. J. Neural Syst.*, vol. 34, no. 3, Mar. 2024, Art. no. 2450010.

[24] L. Meng et al., "Evaluation of decomposition parameters for high-density surface electromyogram using fast independent component analysis algorithm," *Biomed. Signal Process. Control*, vol. 75, May 2022, Art. no. 103615.

[25] D. Farina et al., "Man/machine interface based on the discharge timings of spinal motor neurons after targeted muscle reinnervation," *Nature Biomed. Eng.*, vol. 1, no. 2, p. 0025, Feb. 2017.

[26] N. Rubin, Y. Zheng, H. Huang, and X. Hu, "Finger force estimation using motor unit discharges across forearm postures," *IEEE Trans. Biomed. Eng.*, vol. 69, no. 9, pp. 2767–2775, Sep. 2022.

[27] R. Roy, Y. Zheng, D. G. Kamper, and X. Hu, "Concurrent and continuous prediction of finger kinetics and kinematics via motoneuron activities," *IEEE Trans. Biomed. Eng.*, vol. 70, no. 6, pp. 1911–1920, Jun. 2023.

[28] Y. Zheng and X. Hu, "Interference removal from electromyography based on independent component analysis," *IEEE Trans. Neural Syst. Rehabil. Eng.*, vol. 27, no. 5, pp. 887–894, May 2019.

[29] Y. Zheng and X. Hu, "Concurrent estimation of finger flexion and extension forces using motoneuron discharge information," *IEEE Trans. Biomed. Eng.*, vol. 68, no. 5, pp. 1638–1645, May 2021.

[30] M. Chen and P. Zhou, "A novel framework based on FastICA for high density surface EMG decomposition," *IEEE Trans. Neural Syst. Rehabil. Eng.*, vol. 24, no. 1, pp. 117–127, Jan. 2016.

[31] Y. Ning, X. Zhu, S. Zhu, and Y. Zhang, "Surface EMG decomposition based on K-means clustering and convolution kernel compensation," *IEEE J. Biomed. Health Informat.*, vol. 19, no. 2, pp. 471–477, Mar. 2015.

[32] Y. Chen, C. Dai, and W. Chen, "Cross-comparison of EMG-to-force methods for multi-DoF finger force prediction using one-DoF training," *IEEE Access*, vol. 8, pp. 13958–13968, 2020.

[33] H. Mao, P. Fang, and G. Li, "Simultaneous estimation of multi-finger forces by surface electromyography and accelerometry signals," *Biomed. Signal Process. Control*, vol. 70, Sep. 2021, Art. no. 103005.

[34] L. Meng and X. Hu, "Unsupervised neural decoding for concurrent and continuous multi-finger force prediction," *Comput. Biol. Med.*, vol. 173, May 2024, Art. no. 108384.

[35] C. Chen and X. Zhu, "Tracking motor unit discharges across days based on the pre-trained separation vectors," in *Proc. 10th IEEE RAS/EMBS Int. Conf. Biomed. Robot. Biomechatronics (BioRob)*, Sep. 2024, pp. 681–686.

[36] C. Dai and X. Hu, "Finger joint angle estimation based on motoneuron discharge activities," *IEEE J. Biomed. Health Informat.*, vol. 24, no. 3, pp. 760–767, Mar. 2020.

[37] Y. Zheng and X. Hu, "Concurrent prediction of finger forces based on source separation and classification of neuron discharge information," *Int. J. Neural Syst.*, vol. 31, no. 6, Jun. 2021, Art. no. 2150010.

[38] Y. Zheng and X. Hu, "Muscle activation pattern elicited through transcutaneous stimulation near the cervical spinal cord," *J. Neural Eng.*, vol. 17, no. 1, Feb. 2020, Art. no. 016064.